Cite this: *Analyst*, 2012, **137**, 5302

www.rsc.org/analyst

PAPER

Analysis of protein expression in developmental toxicity induced by MeHg in zebrafish†

Susana Cuello,[a] Pilar Ximénez-Embún,[b] Isabel Ruppen,[b] Helia B. Schonthaler,[c] Keith Ashman,[d] Yolanda Madrid,[a] Jose L. Luque-Garcia*[a] and Carmen Cámara*[a]

Received 5th July 2012, Accepted 12th September 2012
DOI: 10.1039/c2an35913h

Mercury toxicity and its implications in development are a major concern, due to the major threat to ecosystems and human health that this compound represents. Although some of the effects of methylmercury (MeHg) exposure have been extensively studied, the molecular mechanisms of interaction between this compound and developing organisms are still not completely understood. To provide further insights into these mechanisms, we carried out a quantitative proteomic study (iTRAQ) using zebrafish larvae exposed to 5 μg L^{-1} and 25 μg L^{-1} MeHg as a model. In this study, a multidimensional approach combining isoelectric focusing (IEF) and strong cation exchange (SCX) followed by reversed phase liquid chromatography prior to MALDI TOF/TOF analysis was employed, which resulted in a substantial increase in proteome coverage. Among the proteins identified, 71 were found de-regulated by more than 1.5-fold, and implicated in embryonic development, protein synthesis, calcium homeostasis and energy production. Furthermore, morphological and histological analysis of exposed larvae was carried out, reflecting changes such as smaller swim bladder, remaining yolk, bent body axis and accumulation of blood in the heart, among others.

Introduction

Toxicity, biochemical behavior and transport of mercury in the environment are clearly dependent on its chemical form.[1] Inorganic mercury (Hg^{2+}) and monomethylmercury (CH_3Hg^+) are the two most abundant species found in biological samples.[2] It is well known that organomercurial compounds are more harmful than inorganic mercury; however, the latter can also be biomethylated by aquatic organisms, thus making fish consumption the major source of methylmercury for humans.[3] Application of the bioconcentration test 305 (proposed as a standard method by the OECD to adult fish exposed to methylmercury) has demonstrated the high capacity of this compound to be accumulated.[4] Although the bioconcentration factor provides valuable information about the bioaccumulative properties of a chemical, additional information on the mechanisms of interaction and the effects caused in living organisms are required to evaluate the toxicity of a given compound. In our case, it is known that ingested mercury can interact with proteins and enzymes due to its strong affinity for sulfur, causing organ dysfunction and a devastating effect on the whole central nervous system, particularly the developing brain.[5] The generation of reactive oxygen species (ROS) by MeHg as well as the active involvement of the mitochondria in the process have been shown in previous studies.[6,7] Specific proteins and mechanisms related to methylmercury-induced cell death[7] and neurotoxicity[8,9] have also been reported using different biochemical approaches. However, a deeper insight into the mechanisms by which methylmercury exerts its toxicity, particularly during embryonic development, would be highly desired.

Quantitative proteomics appears as a suitable tool for this purpose since hundreds of proteins can be analyzed in a single experiment,[10] thus allowing the identification of those with an altered expression induced by MeHg. These proteins would represent not only potential targets for the study of specific mechanisms by additional biochemical methods, but also as potential biomarkers of MeHg ecotoxicity. The application of advanced proteomic strategies to the toxicological field has been very discrete so far; although in other fields, quantitative proteomics is emerging as a reference exploratory technique.[11,12] As for the study of MeHg-induced toxicity, proteomics has only been applied using gel-based approaches,[13,14] which have important limitations regarding the number of potential identifications.

[a]*Department of Analytical Chemistry, Faculty of Chemistry, Complutense University of Madrid, 28040 Madrid, Spain. E-mail: jlluque@quim.ucm.es; ccamara@quim.ucm.es; Fax: +34 913944329; Tel: +34 913944318*
[b]*Proteomics Core Unit, Spanish National Cancer Research Center (CNIO), Madrid, Spain*
[c]*BBVA Foundation – CNIO Cancer Cell Biology Programme, Spanish National Cancer Research Center (CNIO), Madrid, Spain*
[d]*UQ Centre for Clinical Research, Building 71/918 RBWH, Herston, QLD 4029, Australia*

† Electronic supplementary information (ESI) available. See DOI: 10.1039/c2an35913h

Based on all of the above, we have selected a state-of-the-art quantitative proteomic approach as a discovery strategy, that circumvents the limitations of gel-based proteomic approaches, in order to identify target proteins associated with the mechanisms involved in the developmental toxicity induced by MeHg as well as potential biomarkers of ecotoxicity. iTRAQ[15] (isobaric tags for relative and absolute quantification) was used as the unbiased quantitative proteomic approach in this study. This method allows isotopic labeling of different tissue samples and thus, protein quantitation of up to 8 samples simultaneously in a single experiment.[16] The use of bioinformatic tools also allowed us to identify the biological processes and functions affected upon MeHg exposure. We have selected zebrafish larvae as a model since it has been recently proposed as an alternative to adult fish in the previous OECD test guideline because of the drastic time reduction in the bioaccumulation test (72 hours *vs.* 42 days when using adult fish) and other additional advantages such as (i) sample availability (each female is capable of laying 200–300 eggs per week), (ii) fast embryonic development and (iii) a high similarity on the protein level compared to humans (mostly protein homology is above 70%). This makes it a very suitable model for proteomic analysis of MeHg effects in vertebrates.

In our work, we have evaluated changes in the proteome of zebrafish larvae exposed to 5 and 25 μg L^{-1} of MeHg as compared to control samples. The criteria for selecting 5 and 25 μg L^{-1} exposure concentrations is based on previous experiments done by increasing MeHg levels of exposure. The selected levels allow the observation of changes in the zebrafish embryo within a reasonable time for the assay and without promoting mortality among zebrafish embryo (A LC50 of 250 μg L^{-1} has been reported for MeHg for zebrafish embryo).[17] The results obtained from the proteomic approach, have been supported by morphological and histological analysis carried out on the MeHg-exposed larvae; thus helping to gain a deeper insight into the developmental toxicity induced by MeHg.

Materials and methods

Sample preparation

Zebrafish (*Danio rerio*) larvae (WIK strain) were kindly provided by the Spanish National Cardiovascular Research Center (CNIC, Madrid, Spain). Exposure media were prepared in order to have a similar composition to fresh river water, containing 46.4 mg L^{-1} of $CaCl_2$, 275.2 mg L^{-1} of NaCl, 12.2 mg L^{-1} of KCl and 78.4 mg L^{-1} of $MgSO_4$. Based on OECD guidelines, the culture conditions in this medium were: 26 ± 2 °C, dissolved oxygen ≥ 60% and pH 6–8.5 (before and after renewal). MeHgCl standard solutions used for exposure tests were prepared in culture media daily by making appropriate dilutions of MeHgCl stock standard solution at 1000 mg L^{-1} prepared in methanol. The stock solution was stored in the dark at −18 °C. Zebrafish larvae at 72 h post-fertilization (hpf) were exposed to MeHg for 72 hours in Petri dishes containing different concentrations of MeHg (0 μg L^{-1}, 5 μg L^{-1} and 25 μg L^{-1}), after which the larvae (6 days post-fertilization – 6 dpf) were collected and prepared for the proteomic study or for the microscopic and histological analysis. To avoid potential variability associated with the use of different Petri dishes for each condition, the samples used were pools of larvae grown in different dishes. Concentrations of MeHg in larvae after 72 h of exposure were estimated applying the bioaccumulation factor (BCF) previously calculated by ICP-MS in similar samples at similar exposure times.[8] Considering a BCF value of 2500, the concentration of MeHg in larvae should be around 12.5 μg g^{-1} and 62 μg g^{-1}, for larvae exposed to 5 and 25 μg L^{-1}, respectively.

Protein extraction and peptide labeling

Zebrafish larvae (20 per condition) were resuspended in 200 μL of ice-cold RIPA buffer (20 mM Tris–HCl pH 7.4, 37 mM NaCl, 2 mM EDTA, 1% Triton X-100, 10% glycerol, 0.1% SDS and 0.5% Na deoxycholate) containing protease and phosphatase inhibitors. Samples were incubated on ice for 15 min and centrifuged at 4 °C and 16 000*g* for 10 min. This step was repeated twice and supernatants containing the protein fraction were cleaned-up by acetone precipitation with six volumes of ice-cold acetone. Pellets were dissolved in 0.5 M triethylammonium bicarbonate (TEAB). For the 4-plex iTRAQ experiments, zebrafish larvae from the same genetic background (WIK, wild type strain previously established) were either used as controls or exposed to 5 and 25 μg L^{-1} of MeHg for 72 hours. Biological replicates were carried out with larvae from different matings at different times and in different Petri dishes. Protein concentration was determined by the Bradford assay using BSA as standard. Protein digestion and iTRAQ labeling was performed according to the manufacturer's protocol (Applied Biosystems) and as described elsewhere.[18] Each tryptic digest was labeled with one isobaric amine-reactive tag as follows: Tag_{114} – Control 1, Tag_{115} – Control 2, Tag_{116} – 5 μg L^{-1} MeHg and Tag_{117} – 25 μg L^{-1} MeHg. Labeling was done in two sets of samples in order to obtain two biological replicates (A and B).

Strong cation exchange and OFFGEL fractionation

One half of the sample, equivalent to 50 μg of protein was separated by strong cation exchange chromatography (SCX) as in previous studies.[19] pI-based peptide separation was performed by a 3100 OFFGEL Fractionator System (Agilent Technologies, Böblingen, Germany) with a 24-well set-up. The 24 cm long IPG gel strips (GE Healthcare, München, Germany) with a 3–10 linear pH range were rehydrated for 15 min with the Peptide IPG Strip Rehydradation Solution according to the manufacturer's protocol. Subsequently, 150 μL of the sample was loaded in each well. Isoelectrofocusing (IEF) of the peptides was performed at 20 °C and 50 μA until the 50 kV h level was reached. After focusing, the 24-peptide fractions were withdrawn and the wells rinsed with 100 μL of a solution of water–methanol–formic acid (49/50/1). Rinsing solutions were pooled after 15 min with their corresponding peptide fractions. All fractions were evaporated by centrifugation under vacuum and reconstituted in 0.1% TFA 3% ACN prior to clean up. Solid phase extraction and salt removal was performed with home-made columns based on Stage Tips with C8 Empore Disks (3M, Minneapolis, MN) filled with R2 resin (Applied Biosystems). The bound peptides were washed with 0.1% TFA and eluted with 0.1% TFA 70% ACN. Eluates were evaporated to dryness and maintained at 4 °C.

Reversed-phase liquid chromatography

Each fraction from the SCX or IEF separation was resuspended in 0.1% TFA 3% ACN buffer and separated on an Ultimate 3000 nano-LC system (Dionex-LC Packings, Amsterdam, The Netherlands) equipped with a Probot™ MALDI spotting device (Dionex-LC Packings). In order to pre-concentrate and desalt the samples before switching the pre-column in line with the separation column, 20 μL from each dissolved SCX and IEF fraction was loaded onto a reversed-phase Monolithic PS-DVB 200 μm ID × 5 mm peptide trapping cartridge (Dionex-LC Packings), and washed for 8 min at 20 μL min^{-1} with loading buffer (0.05% HFBA). The peptides were eluted from a RP Monolithic PS-DVB column 200 μm ID × 5 cm analytical column (Dionex-LC Packings) by application of a binary gradient with a flow rate of 2.5 μL min^{-1}. Buffer A was 2% ACN in 0.05% TFA, buffer B was 50% ACN with 0.04% TFA. The gradient used was 0–8 min 0% B, 8–39 min 65% B, 39–45 min 90% B and 45–55 min 0% B. For IEF fractions, 2% of buffer B was used during the washing step and column equilibration. The column effluent was mixed directly with the MALDI matrix solution (3 mg mL^{-1} α-cyano-4-hydroxycinnamic acid in 70% ACN with 0.1% TFA) at a flow rate of 2.5 μL min^{-1} through a μ-Tee connection, before spotting onto 1664-well stainless steel MALDI target plates (Applied Biosystems) using a Probot micro fraction collector (Dionex-LC Packings) with a speed of 5 s per well. The matrix contained 10 mM $NH_4H_2PO_4$ and 10 nmol of P14R synthetic peptide (monoisotopic $(M + H)^+ = 1533.8582$; $C_{76}H_{113}N_{18}O_{16}$) (Sigma, St. Louis, MO, USA) as an internal standard for mass calibration.

Protein identification and quantification by mass spectrometry

MALDI target plates were analyzed using a 4800 Analyzer equipped with TOF/TOF ion optics (ABSCIEX. Concord, Ontario, Canada), and 4000 Series Explorer software version 3.5.1. as described elsewhere.[18] Protein identification and relative quantification were performed with the ProteinPilot™ software (version 3.0; ABSCIEX) using the Paragon™ algorithm as described in detail in the ESI† "Protein ID/QT Methods". Precursor and fragment ion mass tolerance were set to 0.2 and 0.4 Da, respectively. The results were then exported into Excel for manual data interpretation. Although relative quantification and statistical analysis were provided by the ProteinPilot 3.0 software, an additional 1.5-fold change cutoff for all iTRAQ ratios was selected to classify proteins as up- or down-regulated.

Statistical analysis

The relative protein levels between the iTRAQ-labeled samples were estimated based on the quantitative ratios. The average ratio for each protein was calculated by ProteinPilot™ based on the ratio values for each peptide. These values were determined based on the peak area ratios on the MS/MS spectra between ions *m*/*z* 114.1, 115.1, 116.1 and 117.1 (corresponding to the different iTRAQ tags). ProteinPilot™ also provided the *P*-value for each protein, which measures the certainty that the average ratio differs from 1. The smaller the *P*-value, the more likely any differential expression observed is real. Proteins showing a *P*-value <0.05 were considered de-regulated by the ProteinPilot™ software. However, in our experiment, an additional cut-off of 1.5-fold change was selected due to the variability associated with our samples. Further details on the statistical analysis are given in the ESI.†

Bioinformatic-based functional analysis

Protein ID mapping was carried out by the web-free application Protein Identifiers Cross-Reference (PICR) to establish the cellular localization, the biological function and the biological process in which the identified proteins are involved based on Gene Ontology annotations. In order to know potential intracellular signaling pathways or molecules affected by MeHg exposure, the significantly de-regulated proteins with their NCBI accession number and the ratio changes were imported into the Ingenuity Pathway Analysis (IPA) software package (Ingenuity Systems Inc.).

Histological analysis

For histological analyses by light microscopy (LM), larvae were fixed in 4% paraformaldehyde (PFA) in PBS (pH 7.2) at 4 °C overnight and washed three times in PBS. The embryos were dehydrated in a standard ethanol series, infiltrated and embedded in paraffin for sectioning. For H&E staining, 5 μm sections were processed according to standard procedures.

Results and discussion

Combination of SCX and IEF increase proteome coverage

In this study, a multidimensional approach combining IEF and SCX followed by reversed phase liquid chromatography was used for extensive peptide separation (Fig. 1). A total number of 1189 and 1141 proteins were identified by ProteinPilot in biological replicates A and B, respectively, after the overall analysis of all spectra acquired in the study. For further analysis, only proteins identified with 2 or more distinct peptides were considered, resulting in 667 and 594 proteins identified in biological replicates A and B, respectively. A total of 442 identified proteins were common to both biological replicates, showing a significant overlap between samples (Fig. 2A).

Peptide fractionation combining IEF and SCX has been shown to increase protein identification over classic multidimensional approaches such as MudPIT, since three distinct separation techniques are employed. 484 and 350 proteins were identified in replicate A after the analysis of data obtained from SCX and IEF fractionation samples, respectively (Fig. 2B). In replicate B, 389 and 339 proteins were independently identified from SCX and IEF approaches (Fig. 2C). Hence, SCX provided more protein identifications, thus confirming that the degree of proteome coverage is proportional to the extent of peptide fractionation (ESI, Fig. S1†).[19]

Fig. 2B and C also show the overlapping of the fractionation techniques, since only 38% of all the proteins identified in replicate A and 35% of all the proteins identified in replicate B were detected using both approaches.

As a result, we can conclude that the number of proteins identified is significantly high after using complementary techniques for sample fractionation before RP separation, which is the ultimate goal of discovery-oriented experiments.

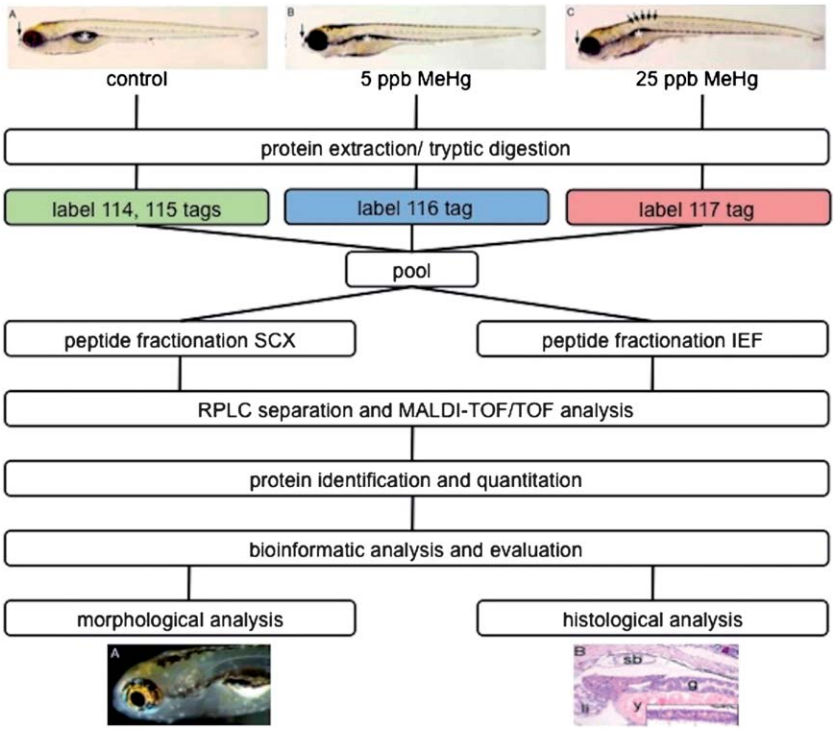

Fig. 1 General scheme of the discovery platform used based on iTRAQ in combination with SCX and IEF separation and MALDI-TOF/TOF analysis.

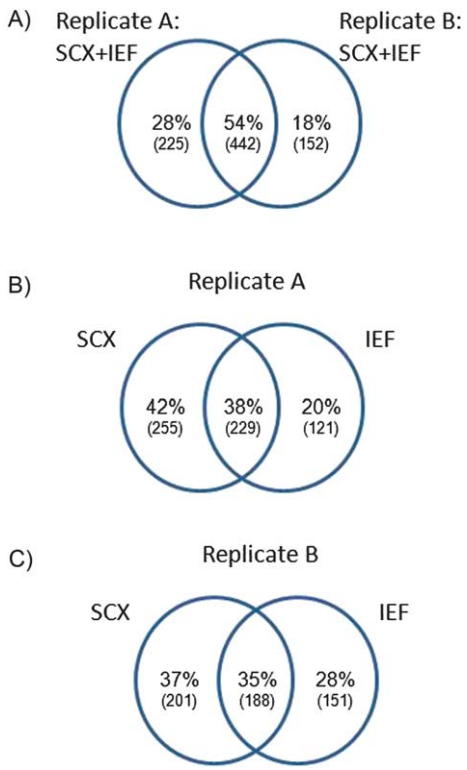

Fig. 2 Venn diagrams depicting the overlap of proteins (A) between replicate A and replicate B when combining spectra from SCX and IEF separations, (B) between SCX and IEF approaches in replicate A and (C) between SCX and IEF approaches in replicate B. Only proteins identified with two or more peptides with 95% confidence were considered.

Protein abundance changes upon MeHg exposure

We analysed the larval zebrafish proteome in two large-scale iTRAQ biological replicates (20 zebrafish larvae per condition). In these experiments control larvae were compared to larvae exposed to 5 μg L^{-1} and 25 μg L^{-1} of MeHg for 72 h. Altogether 819 proteins were identified in the two iTRAQ experiments with two or more unique peptides, which was the criteria considered for valid hits. Using 1.5 as the threshold for a significant fold change due to the expected heterogeneity of the samples, 18 proteins were found de-regulated upon 5 μg L^{-1} MeHg exposure, of which half of the proteins were up-regulated and the other half down-regulated (Table 1). As for the larvae exposed to 25 μg L^{-1} of MeHg, we found 58 de-regulated proteins, from which 42 were up-regulated (Table 2) and 16 down-regulated (Table 3). Detailed information of the de-regulated proteins is provided as ESI (Tables S1 and S2†). As expected, the increase in MeHg concentration was directly correlated with the increase in the number of de-regulated proteins. However, the identified de-regulated proteins were significantly different between larvae treated with the two different MeHg concentrations, thus reflecting differences in the activation of different biological functions due to the treatment. This can be explained by the fact that our study was carried out on a developing organism, which means that the same organs and functions may be affected differently at different concentrations of MeHg due to the different needs of every organ at different developmental stages. These results correlate well with the morphological and histological changes observed (see below) under both conditions. Regarding the iTRAQ ratio distribution, most of the identified proteins were within an iTRAQ ratio close to 1, as expected for a 1 : 1 : 1 : 1 mixture.

Table 1 Proteins found de-regulated in 6 dpf zebrafish larvae exposed to 5 μg L^{-1} of MeHg

Accession number (gi)	Common name	Protein name	Average iTRAQ ratio	iTRAQ ratio A	*P*-value A	Number of peptides A	iTRAQ ratio B	*P*-value B	Number of peptides B
47550733	serbp1	SERPINE1 mRNA binding protein 1	2.91	NQ	NQ	NQ	2.91	0.018	5
18858587	eef1a	Elongation factor 1-alpha	2.13	2.52	0.608	4	1.74	0.021	6
18858197	gstp1	Glutathione S-transferase pi[a]	1.76	1.70	0.002	8	1.82	0.004	6
18859297	pvalb2	Parvalbumin-2[a]	1.68	1.65	0.001	5	1.71	0.011	4
157787181	ckmb	Muscle creatine kinase b	1.66	1.72	0.007	5	1.60	0.208	2
33636707	pvalb9	Parvalbumin 9[a]	1.62	1.62	0.051	3	NQ	NQ	NQ
55742597	eif5a2	Eukaryotic translation initiation factor 5A-2	1.59	1.54	0.253	2	1.64	0.474	3
31795559	tnnt3b	Troponin T3b, skeletal, fast isoform 2	1.54	1.58	0.008	5	1.50	0.026	5
18858947	krt4	Keratin 4	1.54	1.67	0.014	7	1.41	0.979	4
113678458	vtg2	Vitellogenin 2 isoform 1	−1.54	−1.54	0.001	20	−1.54	0.001	23
156713467	vtg7	Vitellogenin 7	−1.56	−1.54	0.079	6	−1.58	0.014	10
68448530	vtg5	Vitellogenin 5	−1.56	−1.43	0.074	11	−1.69	0.001	15
189523697	ttnb	Titin b	−1.56	NQ	NQ	NQ	−1.56	0.037	6
303227889	vtg6	Vitellogenin 6	−1.59	−1.55	0.059	5	−1.63	0.008	9
68444085	mfap4	Microfibrillar-associated protein 4-like	−1.79	NQ	NQ	NQ	−1.79	0.026	2
66472252	smyhc1	Slow myosin heavy chain 1	−1.85	−1.95	0.022	3	−1.75	0.045	7
189523699	ttna	Titin a[a]	−2.38	NQ	NQ	NQ	−1.32	0.359	6
238776848	myhz1.2	Myosin, heavy polypeptide 1.2[a]	−3.85	−3.85	0.0020	11	NQ	NQ	NQ

[a] Proteins de-regulated at both 5 and 25 ppb of MeHg exposure.

Functional analysis

The functional annotation of the 71 differentially expressed proteins in control *vs.* MeHg exposed larvae was assigned using the web-free application Protein Identifiers Cross-Reference (PICR) based on the Gene Ontology database. Three main types of annotations were obtained: the cellular compartment, the molecular function and the biological process (Fig. 3). A high number of de-regulated proteins (32%) were localized in the cytosol and the cytoskeleton, supporting the relevance of these compartments in the mechanisms involved in MeHg-induced toxicity (Fig. 3A). The ontology analysis indicated the relevance and diversity of molecular functions of these proteins, such as catalytic activity (34%), nucleotide binding (16%) and transport activity (11%) (Fig. 3B). The data in Fig. 3C are supported by previous studies on the impact of MeHg exposure[11–13] since several biological processes that appeared to be de-regulated proteins include the metabolic process (32%), transport (14%) and response to stimulus (14%). Moreover, we identified processes that are closely related to methylmercury toxicity, such as developmental processes (4%) and apoptosis (9%). The data identifying de-regulated proteins were further analyzed using the IPA software to scrutinize for key biological processes and pathways of relevance regarding the mechanisms of toxicity associated with MeHg. In addition, the software was used to statistically rank the various pathways in order of significance. Therefore, 58 ID proteins were imported into the software and 38 were mapped by the knowledge database functions among those proteins included cellular assembly and organization, including formation of filaments (si:dkey-46g23.2, fn1b, krt18, pfn2l, ttnb), gastrointestinal disease, hepatic system disease including damage of liver (c3, krt18, krt8) and neurological disease, with sub-functions such as movement disorders and neuromuscular diseases (si:dkey-46g23.2, AK1, c3, gstp1, nme2b.1, pfn2l, rpia, uchl1). The most relevant functions associated with the top network generated from the analysis (ESI, Fig. S2†) include cellular assembly and organization; cellular function and maintenance; and cellular movement. These data are consistent with the morphological and histological alterations observed in exposed larvae, and with the well-known neurotoxic[20–22] and hepatotoxic[7,23] properties of MeHg.

In order to correlate both the proteomic results and the histological observations with the functional analysis, we used the databases ZFin (http://zfin.org)[24] and ZF-Espresso (http://zf-espresso.tuebingen.mpg.de/). These repositories contain *in situ* hybridation studies showing organ-specific expression patterns. References supporting the organ-specific location of proteins found deregulated upon MeHg exposure are included as ESI (Table S3†).

Histological analysis

6 dpf control larvae showed the typical developmental morphology at this developmental stage (Fig. 4A), whereas 6 dpf zebrafish larvae exposed to 5 μg L^{-1} (Fig. 4B) and 25 μg L^{-1} (Fig. 4C) showed a significantly smaller swim bladder (not macroscopically visible) (ESI, Fig. S3†) and a morphological change of the upper jaw (flattening of the anterior part), this was more pronounced in larvae exposed to the higher concentration. Moreover, these larvae showed a bent body axis above the trunk region (see arrows in Fig. 4C). Previous studies where embryos of fathead minnow,[25] killfish[26] and zebrafish[27] were exposed to different concentrations of Hg showed similar features including

Table 2 Up-regulated proteins in 6 dpf zebrafish larvae exposed to 25 μg L^{-1} of MeHg

Accession number (gi)	Common name	Protein name	Average iTRAQ ratio	iTRAQ ratio A	*P*-value A	Number of peptides A	iTRAQ ratio B	*P*-value B	Number of peptides B
189521249		Hypothetical protein	15.10	16.28	0.025	4	13.92	0.136	4
24308537	zp2.4	Zona pellucida glycoprotein 2.4	7.44	NQ	NQ	NQ	7.44	0.029	9
47086603	si:dkeyp-50f7.2	ZPA domain containing protein isoform 2	7.76	7.76	0.017	7	NQ	NQ	NQ
41055329	chia	Acidic chitinase	6.04	6.42	0.009	5			1
94536701	si:dkeyp-50f7.2	ZPA domain containing protein isoform 1	6.04	NQ	NQ	NQ	6.04	0.011	5
125816799	si:dkey-46g23.2	si:dkey-46g23.2	5.83	7.58	0.004	3	4.08	0.003	5
61651682	fn1b	Fibronectin 1b	3.65	3.65	0.038	6	NQ	NQ	NQ
226442998	he1b	Hatching enzyme 1b	3.12	NQ	NQ	NQ	3.12	0.004	1
288856329	myhz1.1	Myosin, heavy polypeptide 1.1	3.05	2.85	0.008	13	3.25	0.001	4
238776848	myhz1.2	Myosin, heavy polypeptide 1.2[a]	2.30	NQ	NQ	NQ	2.30	0.021	13
50355968	calrl	Calreticulin like	2.15	2.15	0.074	5	NQ	NQ	NQ
41054259	pdia4	Protein disulfide-isomerase A4	2.14	2.07	0.132	7	2.21	0.365	5
82658290	hmgb2	High-mobility group box 2	2.11	2.11	0.029	5	NQ	NQ	NQ
292610077	c3	Complement component 3	2.08	1.87	0.178	4	NQ	NQ	NQ
53749651	ppib	Peptidyl-prolyl *cis–trans* isomerase B	2.06	2.07	0.017	6	2.05	0.009	5
18858197	gstp1	Glutathione S-transferase pi[a]	2.05	1.91	0.002	8	2.19	0.209	6
18859107	nme2b.1	Nucleoside diphosphate kinase A	2.01	1.94	0.005	4	2.08	0.087	4
125827065	si:dkey-88l16.3	si:dkey-88l16.3	1.98	1.98	0.039	2	NQ	NQ	NQ
33636707	pvalb9	Parvalbumin 9[a]	1.95	1.97	0.230	3	1.93	0.346	3
292618718	vtg3	Vitellogenin 3, phosvitinless	1.86	1.86	0.006	19	NQ	NQ	NQ
40254675	lmnb1	Lamin-B1	1.84	1.84	0.406	5	NQ	NQ	NQ
189523699	ttna	Titin a[a]	1.83	NQ	NQ	NQ	1.83	0.592	6
82524272	c3b	Complement component c3b	1.81	NQ	NQ	NQ	1.81	0.005	2
189535920	flna	filamin A, alpha	1.80	2.07	0.002	19	1.53	0.758	16
41393111	uchl1	Ubiquitin carboxyl-terminal hydrolase isozyme L1	1.79	1.72	0.009	4	1.86	0.505	2
292619135	flnb	Filamin B, like, partial	1.78	NQ	NQ	NQ	1.78	0.009	3
30410758	krt18	Keratin, type I cytoskeletal 18	1.73	1.73	0.039	3	NQ	NQ	NQ
67972636	hnrnpab	Heterogeneous nuclear ribonucleoprotein A/B	1.72	1.65	0.273	2	1.79	0.027	2
18859297	pvalb2	Parvalbumin-2[a]	1.62	1.52	0.002	5	1.72	0.007	4
56118638	pfn2l	Profilin-2	1.62	1.62	0.005	2	NQ	NQ	NQ
41151982	mvp	Major vault protein	1.60	1.39	0.045	6	1.81	0.049	6
65301457	prdx3	Thioredoxin-dependent peroxide reductase, mitochondrial	1.57	1.57	0.119	2	NQ	NQ	NQ
48597012	rpl23a	60S ribosomal protein L23a	1.57	1.44	0.034	3	1.70	0.005	1
41152461	rpl7a	60S ribosomal protein L7a	1.56	1.56	0.084	1	NQ	NQ	NQ
41386743	eef2b	Eukaryotic translation elongation factor 2b	1.56	1.56	0.080	8	NQ	NQ	NQ
292611632	BX901973.4	Hypothetical protein LOC325896	1.56	1.44	0.043	4	1.68	0.007	5
68442739	his4r	Histone H4 replacement-like	1.55	1.48	0.096	5	1.62	0.003	2
41053774	erp44	Endoplasmic reticulum resident protein 44	1.54	1.54	0.226	3	NQ	NQ	NQ

[a] Proteins de-regulated at both 5 and 25 ppb of MeHg exposure.

flexure of the embryonic axis,[25] increase of the spinal curvature[26] and abnormalities along the finfold,[27] which is consistent with the fact that some of the proteins found de-regulated in our study were located in the musculature system (ESI, Table S3†). Other organs such as brain, ear and liver seemed to be affected by MeHg exposure as compared to control larvae that showed typical developmental morphology (Fig. 4D). The fold between the telencephalon and the tectum was absent in larvae exposed to 5 μg L^{-1} MeHg and a slight hammerhead was observed (Fig. 4E). These changes were even more dramatic in the zebrafish larvae exposed to 25 μg L^{-1} (Fig. 4F). In addition, in the larvae exposed to 25 μg L^{-1} MeHg the shape of the ear was irregular and the liver size was increased. Proteins including *c3*, *gstp1*, *c3b* and *rbp4*, that are located in the liver showed an alteration in their expression levels after MeHg exposure (ESI, Table S3†). Larvae exposed to 25 μg L^{-1} also showed an accumulation of blood in the heart region (indicated by an arrow), thus suggesting a possible defect in the cardiac output (Fig. 4F). Devlin and Mottet[28] have previously observed that embryos exposed to MeHg presented abnormalities associated with the circulatory system: the heartbeat was irregular and blood could not make a complete circuit through the heart without difficulty. This observation may be related to the overexpression suffered by the nucleoside diphosphate kinase A, located in the heart, upon MeHg exposure (ESI, Table S3†).

Morphological and histological analyses of the eye did not reveal obvious changes after treatment with either 5 μg L^{-1} or 25 μg L^{-1} MeHg (ESI, Fig. S4†). 6 dpf old zebrafish larvae under

Table 3 Down-regulated proteins in 6 dpf zebrafish larvae exposed to 25 μg L^{-1} of MeHg

Accesion number (gi)	Common name	Protein name	Average iTRAQ ratio	iTRAQ ratio A	*P*-value A	Number of peptides A	iTRAQ ratio B	*P*-value B	Number of peptides B
41152439	rpl10a	60S ribosomal protein L10a	−1.49	−1.49	0.055	3	NQ	NQ	NQ
71834286	apobl	Apolipoprotein B, like	−1.54	−1.44	0.142	46	−1.64	0.242	47
292619319	rbp4	Retinol-binding protein 4, plasma-like	−1.54	NQ	NQ	NQ	−1.54	0.014	2
45387573	pvalb1	Parvalbumin isoform 1d	−1.54	−1.58	0.037	3	−1.50	0.036	2
51571925	AK1	Adenylate kinase isoenzyme 1	−1.56	−1.54	0.063	4	−1.58	0.229	3
48762657	eno1	Alpha-enolase	−1.59	NQ	NQ	NQ	−1.59	0.009	2
54261787	ilf2	Interleukin enhancer-binding factor 2	−1.61	−1.72	0.163	3	−1.50	0.054	5
292617604	crygc	Crystallin, gamma C-like	−1.64	−1.50	0.219	1	−1.69	0.017	2
18858425	krt5	Keratin 5	−1.67	NQ	NQ	NQ	−1.67	0.011	3
41054746	gatm	Glycine amidinotransferase, mitochondrial	−1.69	−1.69	0.106	2	NQ	NQ	NQ
47550793	nnt	NAD(P) transhydrogenase, mitochondrial	−2.08	−2.08	0.109	4	NQ	NQ	NQ
33504543	atp6v1ba	V-type proton ATPase subunit B	−2.13	NQ	NQ	NQ	−2.13	0.065	2
62632719	hbbe3	Hemoglobin beta embryonic-3	−2.22	−2.32	0.049	4	−2.12	0.033	3
27545277	eef1g	Elongation factor 1-gamma	−2.44	−2.08	0.084	6	−2.80	0.127	7

incident light conditions showed the typical pattern and intensity of iridophores in the eye and in the body. Shape and size of the eye was found to be wild-type-like (ESI, Fig. S4a†). 6 dpf zebrafish larvae exposed to 5 μg L^{-1} and 25 μg L^{-1} MeHg displayed a slight reduction of iridophores in the eye (ESI, Fig. S4e and S4f†) and in the body. However, no differences in melanocyte pigmentation or melanin distribution were observed (data not shown). Furthermore, no difference in shape and size of the eye or the pupil were detected in MeHg exposed larvae as compared to controls. This was confirmed by histological analyses (data not shown).

Zebrafish larvae exposed to 25 μg L^{-1} displayed a significantly smaller swim bladder (sb) (Fig. 5). The remaining yolk (y) at this age indicated a developmental delay of the exposed larvae, which is also supported by previous studies where a delay in development was observed due to MeHg and $HgCl_2$ treatment.[28–30] Liver (li) cells showed increased vesicular areas which might indicate an increased liver cell size and disturbed liver cell function (Fig. 5B). The inset in B shows a magnification of the gut (g) where cells containing big vacuoles appeared after exposure. Zebrafish larvae exposed to 25 μg L^{-1} developed a defect in the myotomes as well as in the notochord (Fig. 5D). Myotomes were smaller in size and the boundaries in-between somites were hardly visible. Myofibers within the myotomes appeared to be loosely packed. The high magnification of the notochord (insert in Fig. 5D) showed a defect in the palisade-like structures of the chondrocytes reflecting the bend body-axis (see also arrows in Fig. 4C). The chondrocytes of the notochord were also affected in coho salmon embryos exposed to MeHg in the study carried out by Devlin and Mottet[28] These dysfunctions probably lead to the abnormal swimming behavior observed in the 25 μg L^{-1} treated zebrafish larvae.

MeHg exposure affects embryonic development

Previous studies have shown that MeHg exposure affects the developmental process of fathead minnow,[28] coho salmon,[31] rainbow trout[32] and carp embryos,[33] causing in all the cases a clear developmental delay as compared to control embryos. These data support our findings using zebrafish, where, as commented before in the histological analysis, a remaining yolk was observed in larvae exposed to 25 μg L^{-1} MeHg.

One of the proteins that appeared clearly up-regulated in larvae exposed to 25 μg L^{-1} MeHg (3-fold compared to control larvae) is *he1b* which plays a crucial role in digesting the chorion during the hatching process of fish.[34] Previous studies have demonstrated that not only mercury[35] but also other heavy metals such as cadmium can affect negatively the hatching process in fish.[36] *Rbp4* appeared down-regulated in zebrafish larvae exposed to 25 μg L^{-1} of MeHg. The inhibition of this protein has been associated with stage-specific malformations of the vitelline vessels, the cranial neural tube, and the eye. Reduced levels of *Rbp4* could be the cause for the morphological and histological alterations, *e.g.* malformation of the jaw and the notochord observed in our MeHg-exposed larvae.[37]

Other proteins related to development and found de-regulated in our experiment were zp2.4 and si:dkeyp-50f7.2. Both of them are associated with the zona pellucida or chorion and showed a significant up-regulation. Degradation of the chorion is a crucial step during development; thus, the presence of high amounts of these proteins in MeHg-exposed larvae as compared to controls, correlates well with the developmental delay observed as these proteins were expected to be down-regulated at this developmental stage.

Alteration of the protein synthesis mechanism due to MeHg exposure

Zebrafish larvae exposed to 25 μg L^{-1} MeHg showed a significant de-regulation of ribosomal proteins such as *rpl32a*, *rpl7a* (up-regulated) and *rpl10a* (down-regulated) involved in protein synthesis. It is known that *rpl7a* can induce apoptosis.[31] Our data suggest that apoptosis associated with methylmercury toxicity might be mediated by *rpl7a*.[32,33] The observed relationship between MeHg and the differential expression of ribosomal proteins in skeletal muscles of zebrafish[38] and hepatic cells[39] have also been previously pointed out. In addition, it has also been demonstrated that a reduced activity in ribosomal proteins may lead to deformation of the brain and body trunk,[40] which correlates well with our results in the histological analysis.

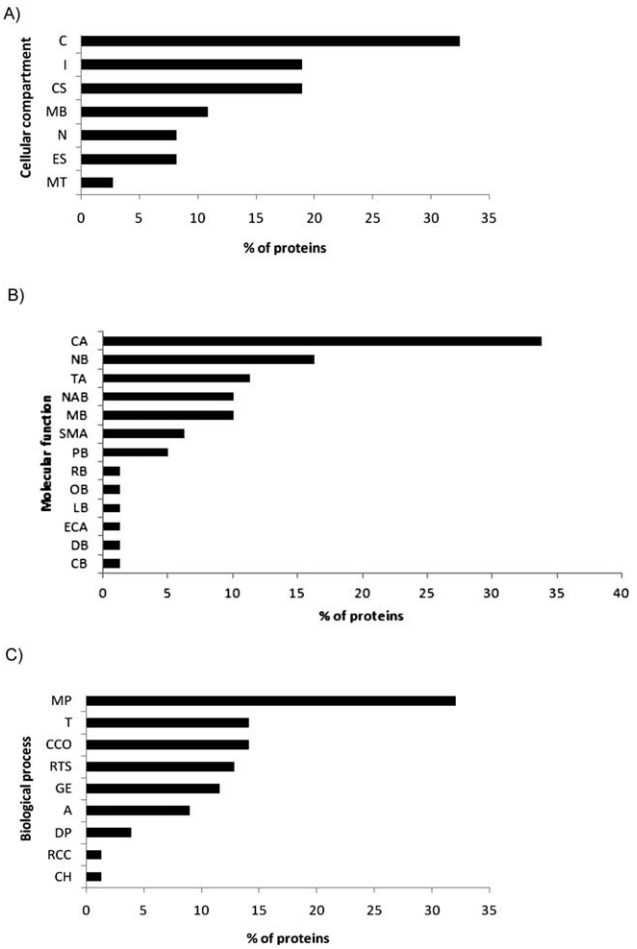

Fig. 3 Classification of the 76 de-regulated proteins according to: (A) cellular compartment. C, cytosol; I, intracellular; CS, cytoskeleton; MB, membrane; N, nucleus; ES, extracellular space; MT, mitochondria. (B) Molecular function. CA, catalytic activity; NB, nucleotide binding; TA, transporter activity; NAB, nucleic acid binding; MB, metal binding; SMA, structural molecule activity; PB, protein binding; RB, ribonucleoprotein binding; OB, oxygen binding; LB, lipid binding; ECA, electron carrier activity; DB, drug binding; CB, carbohydrate binding. (C) Biological process. MP, metabolic process; T, transport; CCO, cellular component organization; RTS, response to stimulus; GE, gene expression; A, apoptosis; DP, developmental process; RCC, regulation of cell cycle; CH, cellular homeostasis.

Other proteins associated with protein synthesis that have been found up-regulated in our study are *eif5a2*, *eef1a* and *hnrnpab*. Recent studies[38] have indicated that *eif5a2* may be involved in apoptotic pathways; in fact, *eif5a2* may have pro-apoptotic functions. *Eef1a* has also been found up-regulated in zebrafish fed with a MeHg-contaminated diet.[38] It is an abundant and ubiquitous cellular protein responsible for the GTP-dependent recruitment of aminoacyl-tRNAs to the ribosome during the elongation cycle of protein translation and it has been implicated in facilitating the apoptosis, being essential for the protein synthesis needed to fuel the machinery required for apoptosis.[38] Our data show that due to MeHg treatment several molecules related to apoptosis are de-regulated suggesting increased cell death in the developing organism due to MeHg treatment.

Calcium homeostasis represents a key mechanism of MeHg-induced toxicity

Calreticulin is a highly conserved multifunctional Ca^{2+} buffering chaperone localized in the lumen of the endoplasmatic reticulum (ER) where it binds to newly synthesized glycoproteins, thus preventing their aggregation and assisting in their correct protein folding.[41] Increased expression of calreticulin results in elevated Ca^{2+} concentrations that cause the ER stress.[42] In a previous study where Atlantic cod was exposed to Hg-enriched sediments, calreticulin was found significantly up-regulated in gills and liver, thus suggesting the potential of this protein as an ecotoxicity marker of exposure to Hg and possibly, to other heavy metals that may interfere with Ca^{2+} homeostasis.[43]

Several parvalbumin proteins such as *pvalb2* and *pvalb9* were up-regulated at the two concentrations of MeHg tested, whereas *pvalb1* was down-regulated at the highest dose of MeHg. Parvalbumins are calcium-binding proteins that have been previously associated with several clinical disorders such as Alzheimer's disease, nervous system disorders, age-related cognitive defects and some forms of cancers,[44] with all of them also related to the toxic effects associated with MeHg exposure. In addition, also supporting this fact, a previous study has shown de-regulation of the genes encoding parvalbumins after exposing zebrafish to MeHg.[30]

It is also important to mention the close relationship existing between the disturbances in calcium homeostasis with the generation of reactive oxygen species (ROS) in the mitochondria,[45] the latter being a well-established effect related to MeHg-induced cell death.[46] The oxidative stress conditions due to MeHg exposure may accelerate protein degradation by autophagy and by the ubiquitin-proteasome system. In fact, several proteins related to lysosomal and autophagic functions such as vitellogenins, V-ATPase, ER proteins and microtubule-associated proteins were found de-regulated in our experiment.

MeHg exposure affects the energy production machinery

Several proteins related to energy production such as *ckmb* and two ATPases (*atp6v1a*, *atp6v1ba*) were found de-regulated after MeHg exposure. The inactivation of ATPases has been related to pathological and physiological abnormalities, and with neurodegenerative diseases.[47] Mercurial compounds, especially MeHg, have been reported to specifically bind this type of enzyme, thus suppressing their activity and causing cellular and organic dysfunction.[48] In addition, the induction of oxidative stress, which is a phenomenon involved in MeHg-induced toxicity, has also been closely related to the inhibition of ATPase activities, supporting our findings.[49]

Other processes affected by MeHg exposure

The results from our iTRAQ experiment, indicate that other proteins may play an important role in the developmental toxicity induced by MeHg and the biological processes implicated are as follows: *flnb*, which is an actin binding protein and have been previously shown to be altered by exposure to most heavy metals such as zinc, arsenic, mercury and cadmium, causing disruption of actin and microtubules in intact cells and thus, affecting the cellular organization.[50] The observed

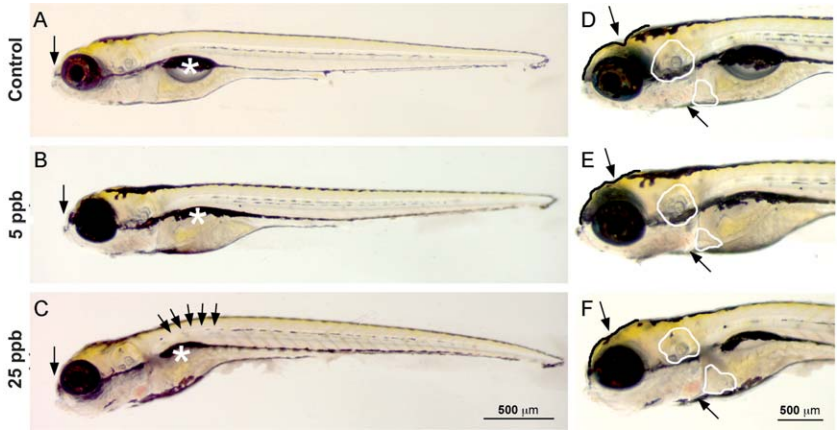

Fig. 4 Zebrafish larvae treated for 3 consecutive days with methylmercury (5 μg L^{-1} and 25 μg L^{-1}) starting at 3 days postfertilization (dpf). (B and C) The swim bladder is indicated by an asterisk and the upper jaw by an arrow. (D–F) The shape of the brain is outlined by a black line and the fold between the telencephalon and the tectum is indicated by an arrow. The ear and the liver are outlined by white lines.

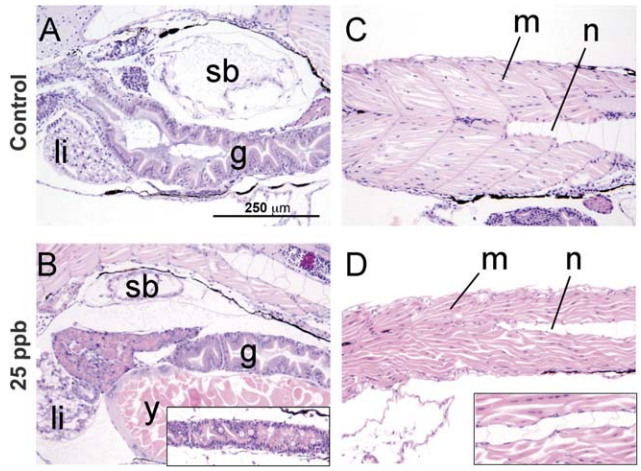

Fig. 5 Histological analysis of 6 dpf zebrafish larvae treated for 3 days with 25 μg L^{-1} methylmercury. (A) Longitudinal section of a 6 dpf zebrafish control larva showing the trunk region. (B) Longitudinal section of a 6 dpf zebrafish treated with 25 μg L^{-1} showing the trunk region. (C) Posterior trunk region of a control 6 dpf zebrafish larva showing the myotomes (m) and the notochord (n). (D) Posterior trunk region of a zebrafish larva treated with 25 μg L^{-1} of MeHg.

increased expression of *Gstp1*, *Prdx3* and *Pdia4* may be induced by the oxidative stress conditions. In the case of *Gstp1*, its up-regulation is consistent with our previous study carried out *in vitro* with HepG2 cells,[7] in which an increased GST activity was observed after 2 h of MeHg exposure and continued increasing up to 24 h. This increased GST activity could be related to the cellular detoxification of MeHg[41] since GST catalyses the reaction of endogenous GSH with xenobiotics to yield less toxic conjugates that are easily eliminated.[51] *Prdx3* is a protein involved in the antioxidant defense system with an active dithiol site which is responsible for the reduction of SH groups in several proteins that have been oxidized under a situation of oxidative stress. In our experiment, *prdx3* appeared up-regulated, thus showing another potential defense mechanism against MeHg toxicity.[52] Another protein found up-regulated in zebrafish larvae exposed to 25 μg L^{-1} MeHg was *mvp*, which is linked to multidrug resistance; in fact, high levels of *mvp* have been found in tissues chronically exposed to xenobiotics. In addition, the expression of *mvp* is correlated with the degree of malignancy in certain types of cancer, suggesting a direct involvement in tumor development and/or progression.[53] *Chia* was one of the proteins found with a high iTRAQ ratio in larvae exposed to the highest concentrations of MeHg. This protein is involved in carbohydrate metabolism and so far has only been shown to be induced in plants exposed to mercury. Moreover, it is known that up-regulation of glutathione S-transferase (gstp1) may induce pathogenesis-related proteins such as chitinase,[54,55] in agreement with our results where both glutathione S-transferase and chitinase (chia) have been found over-expressed. Fibronectin, found up-regulated at 25 ppb MeHg exposure, is a glycoprotein involved in cell adhesion and migration processes including embryogenesis, wound healing, blood coagulation and host defense. *In situ* hybridation studies show specific enrichment of this protein in epidermis (ESI, Table S3†).

Conclusion

We have applied a quantitative proteomic approach for the identification of novel protein targets and pathways associated with the developmental toxicity induced by MeHg in zebrafish. From the methodological point of view, iTRAQ has been combined with two different peptide separation techniques (SCX and IEF) showing a significant increase in the proteome coverage. Our experiments have identified a number of proteins whose expression is altered upon MeHg exposure, thus providing a set of targets closely related to MeHg induced toxicity. This has allowed us for the identification of crucial biological and molecular functions affected by MeHg such as embryonic development, calcium homeostasis, protein synthesis and energy production. Our findings have correlated well with previous studies and have also proposed novel targets for future studies, thus providing a deeper knowledge on the toxicity induced by MeHg in developing organisms. In addition, the morphological and histological analyses of zebrafish larvae have supported the results obtained by our proteomic approach.

Acknowledgements

J.L.L.-G. was financially supported by the "Ramón y Cajal" program from the Spanish Ministry of Science and Innovation. S.C. was supported by a FPU predoctoral fellowship from the Spanish Ministry of Education. P.X.-E. was partially supported by the Spanish National Institute of Health (grant no. CA10/01231). We thank Eduardo Díaz from the Spanish National Cardiovascular Research Center (CNIC) for kindly providing the zebrafish larvae. This work was partially supported by grants CTQ2010-18644 and CTQ2011-28328C02-01 from the Spanish Ministry of Economy and Competitivity and a grant from the *Comunidad de Madrid* (Analisyc II).

References

1 W. Baeyens, *TrAC, Trends Anal. Chem.*, 1992, **11**, 245–254.
2 M. Leemarkers, W. Baeyens, P. Quevauviller and M. Horvat, *TrAC, Trends Anal. Chem.*, 2005, **24**, 383–393.
3 D. S. Forsyth, V. Casey, R. W. Dabeka and A. McKenzie, *Food Addit. Contam.*, 2005, **22**, 535–540.
4 A. V. Weisbrod, L. P. Burkhard, J. Arnot, O. Mekeyan, P. H. Howard, C. Russom, R. Boethling, Y. Sakuratani, T. Traas, T. Bridges, C. Lutz, M. Bonnell, K. Woodburn and T. Pakerton, *Environ. Health Perspect.*, 2007, **115**, 255–261.
5 K. Eto, *Toxicol. Pathol.*, 1997, **25**, 614–623.
6 M. Aschner, T. Syversen, D. O. Souza, J. B. Rocha and M. Farina, *Braz. J. Med. Biol. Res.*, 2007, **40**, 285–291.
7 S. Cuello, L. Goya, Y. Madrid, S. Campuzano, M. Pedrero, L. Bravo, C. Camara and S. Ramos, *Food Chem. Toxicol.*, 2010, **48**, 1405–1411.
8 G. L. Engel, A. Delwig and M. D. Rand, *Toxicol. In Vitro*, 2012, **26**, 485–492.
9 M. Fujimura and F. Usuki, *Toxicol. Sci.*, 2012, **126**, 506–514.
10 K. M. Coombs, *Expert Rev. Proteomics*, 2011, **8**, 631–643.
11 M. Wilm, *Proteomics*, 2009, **9**, 4590–4605.
12 X. H. Li, C. Li and Z. Q. Xiao, *J. Proteomics*, 2011, **74**, 2642–2649.
13 K. Berg, P. Puntervoli, S. Valdersnes and A. Goksoyr, *Aquat. Toxicol.*, 2010, **100**, 51–65.
14 O. J. Nostbakken, S. A. Martin, P. Cash, B. E. Torstensen, H. Amlund and P. A. Olsvik, *Aquat. Toxicol.*, 2012, **108**, 70–77.
15 P. L. Ross, Y. N. Huang, J. N. Marchese, B. Williamson, K. Parker, S. Hattan, N. Khainovski, S. Pillai, S. Dey, S. Daniels, S. Purkayastha, P. Juhasz, S. Martin, M. Bartlet-Jones, F. He, A. Jacobson and D. J. Pappin, *Mol. Cell. Proteomics*, 2004, **3**, 1154–1169.
16 K. Ashman, M. I. Ruppen-Cañas, J. L. Luque-Garcia and F. García-Martínez, Stable Isotopic Labeling for Proteomics, in *Sample Preparation in Biological Mass Spectrometry*, ed. A. R. Ivanov and A. V. Lazarev, Springer Science + Business Media B.V., 2011, pp. 549–573.
17 S. Cuello, J. Sanz-Landaluze, Y. Madrid, J. Guinea and C. Camara, *Talanta*, 2012, **80**, 160–177.
18 I. Ruppen, L. Grau, E. Orenes-Piñero, K. Ashman, M. Gil, F. Algaba, J. Bellmunt and M. Sanchez-Carbayo, *Mol. Cell. Proteomics*, 2010, **9**, 2276–2291.
19 R. J. Slebos, J. W. Brock, N. F. Winters, S. R. Stuart, M. A. Martinez, M. Li, M. C. Chambers, L. J. Zimmerman, A. J. Ham, D. L. Tabb and D. C. Liebler, *J. Proteome Res.*, 2008, **7**, 5286–5294.
20 S. Hussain, A. Atkinson, S. J. Thompson and A. T. Khan, *J. Environ. Sci. Health, Part B*, 1999, **34**, 645–660.
21 X. Ji, W. Wang, J. Cheng, T. Yuan, X. Zhao, H. Zhang and L. Qu, *Environ. Toxicol. Pharmacol.*, 2006, **22**, 309–314.
22 H. Ashour, M. Abdel-Rahman and A. Khodair, *Toxicol. Lett.*, 1993, **69**, 87–96.
23 N. Mori, A. Yasutake and K. Hirayama, *Arch. Toxicol.*, 2007, **81**, 769–776.
24 Y. Bradford, T. Conlin, N. Dunn, D. Fashena, K. Frazer, D. G. Howe, J. Knight, P. Mani, R. Martin, S. A. Moxon, H. Paddock, C. Pich, S. Ramachandran, B. J. Ruef, L. Ruzicka, H. Bauer Schaper, K. Schaper, X. Shao, A. Singer, J. Sprague, B. Sprunger, C. Van Slyke and M. Westerfield, *Nucleic Acids Res.*, 2011, **39**(suppl 1), D822–D829.
25 E. W. Devlin, *Ecotoxicology*, 2006, **15**, 97–110.
26 J. R. Sharp and J. M. Neff, *Mar. Environ. Res.*, 1980, **3**, 195–213.
27 J. C. Samson and J. Shenker, *Aquat. Toxicol.*, 2000, **48**, 343–354.
28 E. W. Devlin and N. K. Mottet, *Bull. Environ. Contam. Toxicol.*, 1992, **49**, 449–454.
29 E. W. Devlin and N. K. Mottet, *Environ. Sci.*, 1991, **1**, 35–46.
30 K. J. Helmcke, T. Syversen, D. M. Miller 3rd and M. Aschner, *Toxicol. Appl. Pharmacol.*, 2009, **240**, 265–272.
31 M. S. Lindström, *Biochem. Biophys. Res. Commun.*, 2009, **379**, 167–170.
32 B. J. Shenker, L. Pankoski, A. Zekavat and I. M. Shapiro, *Antioxid. Redox Signaling*, 2002, **4**, 379–389.
33 J. L. Franco, T. Posser, P. R. Dunkley, P. W. Dickson, J. J. Mattos, R. Martins, A. C. D. Bainy, M. R. Marques, A. L. Dafre and M. Farina, *Free Radical Biol. Med.*, 2009, **47**, 449–457.
34 A. Okada, K. Sano, K. Nagata, S. Yasumasu, J. Othsuka, A. Yamamura, K. Kubota, I. Iuchi and M. Tanokura, *J. Mol. Biol.*, 2010, **402**, 865–878.
35 W. Huang, L. Cao, J. Liu, L. Lin and S. Dou, *Ecotoxicol. Environ. Saf.*, 2010, **73**, 1875–1883.
36 P. Szczerbik, T. Mikolajczyk, M. Sokolowska-Mikolajczyk, M. Socha, J. Chyb and P. Epler, *Aquat. Toxicol.*, 2008, **53**, 36–44.
37 C. Bavik, S. J. Ward and P. Chambon, *Proc. Natl. Acad. Sci. U. S. A.*, 1996, **93**, 3110–3114.
38 S. Cambier, P. Gonzalez, G. Durrieu, R. Maury-Brachet, A. Boudou and J. P. Bourdineaud, *Environ. Sci. Technol.*, 2010, **44**, 469–475.
39 S. Cuello, S. Ramos, Y. Madrid, J. L. Luque-Garcia and C. Camara, *Anal. Bioanal. Chem.*, 2012, **404**, 315–324.
40 T. Uechi, Y. Nakajima, A. Nakao, H. Torihara, A. Chakraborty, K. Inoue and N. Kenmochi, *PLoS One*, 2006, **1**, e37.
41 Y. Y. Qiu and M. Michalak, *Int. J. Biochem. Cell Biol.*, 2009, **41**, 531–538.
42 X. C. Zhang, E. Szabo, M. Michalak and M. Opas, *Int. J. Dev. Neurosci.*, 2007, **25**, 455–463.
43 P. A. Olsvik, M. Brattas, K. K. Lie and A. Goksoyr, *Chemosphere*, 2011, **83**, 552–563.
44 M. S. Cates, M. L. Teodoro and G. N. Phillips, *Biophys. J.*, 2002, **82**, 1133–1146.
45 M. J. Hansson, R. Månsson, S. Morota, H. Uchino, T. Kallur, T. Sumi, N. Ishii, M. Shimazu, M. F. Keep, A. Jegorov and E. Elmér, *Free Radical Biol. Med.*, 2008, **45**, 284–294.
46 P. Kaur, M. Aschner and T. Syversen, *Toxicology*, 2007, **230**, 164–177.
47 S. P. Yu, *Biochem. Pharmacol.*, 2003, **66**, 1601–1609.
48 J. J. Chuu, S. H. Liu and S. Y. Lin-Shiau, *Toxicol. Lett.*, 2007, **169**, 109–120.
49 R. Rodrigo, J. P. Bachler, J. Araya, H. Prat and W. Passalacqua, *Mol. Cell. Biochem.*, 2007, **303**, 73–81.
50 B. Stamova, P. G. Green, Y. Tian, I. Hertz-Picciotto, I. N. Pessah, R. Hansen, X. Yang, J. Teng, J. P. Gregg, P. Ashwood, J. Van de Water and F. R. Sharp, *Neurotoxic. Res.*, 2011, **19**, 31–48.
51 R. Masella, R. Di Benedetto, R. Vari, C. Filesi and C. Giovannini, *J. Nutr. Biochem.*, 2005, **16**, 577–586.
52 J. Gao, Z. R. Zhu, H. Q. Ding, Z. Qian, L. Zhu and Y. Ke, *Neurochem. Int.*, 2007, **50**, 379–385.
53 E. Steiner, K. Holzmann, L. Elbling, M. Micksche and W. Berger, *Curr. Drug Targets*, 2006, **7**, 923–934.
54 W. Maksymiec, *Acta Physiol. Plant.*, 2007, **29**, 177–187.
55 S. Sarowar, Y. J. Kim, E. N. Kim, K. D. Kim, B. K. Hwang, R. Islam and J. S. Shin, *Plant Cell Rep.*, 2005, **24**, 216–224.